Computational analysis of self-similar capillary-driven thinning and pinch-off dynamics during dripping using the volume-of-fluid method

Jelena Dinic, and Vivek Sharma

Citation: Physics of Fluids **31**, 021211 (2019); doi: 10.1063/1.5061715
View online: https://doi.org/10.1063/1.5061715
View Table of Contents: http://aip.scitation.org/toc/phf/31/2
Published by the American Institute of Physics

Physics of Fluids ARTICLE scitation.org/journal/phf

Computational analysis of self-similar capillary-driven thinning and pinch-off dynamics during dripping using the volume-of-fluid method

Cite as: Phys. Fluids 31, 021211 (2019); doi: 10.1063/1.5061715
Submitted: 22 September 2018 • Accepted: 14 November 2018 •
Published Online: 7 January 2019

Jelena Dinic and Vivek Sharma[a]

AFFILIATIONS

Department of Chemical Engineering, University of Illinois at Chicago, Chicago, Illinois 60607, USA

[a]Author to whom correspondence should be addressed: viveks@uic.edu

ABSTRACT

Drop formation and detachment involve large topological changes, including the formation of a fluid neck that thins down due to surface tension-driven flows, and at the neck pinch-off, properties like Laplace pressure display a finite time singularity. Accurately simulating large topological deformations and nonlinearities encountered during drop formation typically makes numerical simulations computationally demanding as resolving small features close to the pinch-off instant requires high resolution and accuracy. In spite of the inherent advantages in tracking interfaces, preserving mass and computational time needed, very few studies utilize the volume-of-fluid (VOF) method for drop formation studies as early practitioners reported convergence problems for fluids with viscosity greater than ten times water viscosity. In this contribution, we utilize the VOF method as implemented in *FLOW-3D* to simulate the prototypical free surface flow of dripping for Newtonian fluids, including viscosity values four orders of magnitude higher than water viscosity. We benchmark the simulated neck shape, neck evolution rate, and break-up length against experiments carried out as a part of this study. The pinch-off dynamics are determined by a complex interplay of inertial, viscous, and capillary stresses, and self-similar scaling laws that are contrasted here against both experiments and simulations often describe the dynamics. We show that the simulated radius evolution profiles match the pinch-off dynamics that are experimentally observed and theoretically predicted for Newtonian fluids for axisymmetric flows. Furthermore, we determine pre-factors for scaling laws, velocity, and deformation fields within thinning necks, and we show that pre-factors, as well as break-up time and length comparable to experiments can be simulated using the VOF method.

I. INTRODUCTION

Surface tension-driven flows and instabilities underlie drop formation and liquid transfer in many applications[1–8] such as coating and printing (inkjet, gravure, etc.),[2–12] spraying and atomization,[6,12–15] formation of emulsions and drop formation in microfluidics,[16–18] and in dispensing non-Newtonian fluids including polymer solutions,[4,10,19–27] foams, emulsions, and suspensions.[27–29] Analytical and numerical analyses of the free surface flows dominated by capillarity are particularly challenging and complex problems: the type and strength of flow determine the shape of the interface, and yet any change in the interfacial curvature itself influences flow through its contribution to Laplace pressure.[1–3,6–9,30,31] Even the simplest method of forming drops by dripping a rheologically simple (or Newtonian) fluid from a nozzle is known to involve a complex interplay of inertial, viscous, and capillary stresses (plus the effect of gravity and iterated stretching for relatively large drops).[1,3,4,32–34] Drop formation and detachment involve large topological changes, including the formation of a fluid neck that thins down to zero in a finite time, and thus properties like Laplace pressure display a finite time singularity.[3,31–33]

Accurately simulating large topological deformations and nonlinearities encountered during drop formation typically makes numerical simulations computationally demanding as resolving small features close to the pinch-off instant requires high resolution and accuracy.[3,7,9,33,35,36] Several volume and surface tracking methods including boundary integral, finite difference, and finite element methods have been utilized for numerical simulations of the drop formation and pinch-off dynamics problems.[1,3,6,7,9,37–39] However, only a countable few studies have explored the problems using the volume-of-fluid (VOF) method.[40,41] The lack of such studies can be traced to papers[9,36] that questioned the capability of the VOF-based techniques to simulate the drop formation process. For instance, Ambravaneswaran *et al.*[36] in 2002 stated that the volume-of-fluid (VOF) based code failed to converge in the work of Zhang[42] and Delametter (cited by Ambravaneswaran *et al.*[36] as a private communication) "when simulating the formation dynamics of liquids having viscosities that exceed that of water merely by a factor of ten" and also failed to simulate satellite drop formation for lower viscosity fluids.

In the present contribution, we take up the challenge of simulating drop formation and detachment for the prototypical flow geometry of dripping using the VOF method with the following goals. We aim to carry out a close comparison of neck radius evolution datasets obtained using numerical simulations of dripping with experiments as well as theoretical models for describing pinch-off dynamics. We aim to check if high viscosity fluids can be simulated, if satellite drop formation can be observed, and if simulated neck shapes, break-up length, and break-up time capture the features observed experimentally. It is well-established that the capillary-driven thinning and pinch-off dynamics of Newtonian fluids asymptotically approach self-similar dynamics such that neck radius R shows inertio-capillary thinning behavior with $R \propto (t_p - t)^{2/3}$ for low viscosity fluids and viscocapillary thinning behavior with $R \propto (t_p - t)$ for relatively high viscosity fluids. The dimensionless ratio of characteristic viscocapillary to inertio-capillary time scales provides a non-dimensional viscosity measure or a dimensionless group called the Ohnesorge number $Oh = \eta/\sqrt{\rho\sigma R_0}$. Here, η, ρ, and σ represent fluid viscosity, density, and surface tension, respectively, while R_0 is the characteristic length scale of the problem. We aim to ascertain if the shape of the neck as well as neck thinning dynamics of simulated profiles compare well with the self-similar scaling laws. In particular, we wish to compare the material dependent proportionality constant for inertio-capillary and viscocapillary behavior. In this contribution, the VOF method embedded in the commercial computational fluid dynamics (CFD) software *FLOW-3D* is utilized for simulating dripping of Newtonian fluids (including water-glycerol mixtures). The current study explores drop formation for Newtonian fluids with viscosity values up to three orders of magnitude higher than the previously determined upper-limit and also checks for satellite drop formation, which has been cited as another limitation. The rationales for using the VOF method, as well as for opting for a commercial implementation of the method, are discussed next.

It is well-established that computational fluid dynamics can offer insights into processability, design of processing equipment, material characterization, flow types and strengths, instability mechanisms, etc., not readily available from experiments.[31,37,43,44] Among the numerical simulation techniques, the boundary integral method (BIM) is limited to irrotational flow in an inviscid drop ($Re \gg 1$) and Stokes flow ($Re \ll 1$),[36] or cases in which Green's function for the examined flow type is known. Thus, BIM is an unsuitable method for analysis of finite Reynolds number (*Re*) flows encountered in various printing techniques. However, Wilkes *et al.*[37] had successfully developed and used a finite element method (FEM) for solving three-dimensional axisymmetric (or 2D) flow during formation of droplets. Eggers and Dupont[35] showed that finite difference method (FDM) models can be used for solving one-dimensional (1D) slender jet problems through numerical approximation by assuming that the radial length scale of the liquid neck is typically much smaller than its longitudinal length scale. However, the FDM model fails to accurately capture thinning dynamics close to pinch-off for low viscosity fluids. Due to the steady progress made in the implementation of the volume-of-fluid (VOF) method over the last few decades, the numerical simulations appear to be particularly suitable for drop formation and detachment as the tracking of interfaces, conservation of mass and momentum, and the topological transitions are handled implicitly within the algorithm.

The success in simulating prototypical flows such as the one of drop formation using the VOF method is desired from the engineering perspective both in terms of understanding processability and printability of fluids for different applications and in terms of exploring fundamental questions related to the mechanics of free surface flows. It can be argued that a computational fluid dynamics platform that is pre-designed with built-in, physically robust features for incorporating fluid properties like surface tension and rheological behavior, substrate or surface properties and interactions with the fluid, and programmable shape and size of equipment or structures could be used for streamlined utilization of computation for solving complex and critical problems. The current study is motivated primarily by the idea of developing a foundational basis for such a platform that would enable, at a later stage, CFD models with highly nonlinear and relatively poorly understood effects (including nonlinear viscoelasticity, as a future goal). Here we limit our attention to Newtonian fluids and benchmark the capabilities of the VOF method by carrying out necessary comparisons with theory and experiments for the two limiting cases of low and high viscosity fluids.

The paper is organized as follows. The first section summarizes how the VOF method embedded in the commercial computational fluid dynamics (CFD) software *FLOW-3D* is utilized to simulate and capture capillary-driven thinning and pinch-off dynamics in the prototypical free surface flow realized during dripping. Numerical simulations of dripping of low viscosity fluids are presented first, and a comparison with experimental studies carried out with glycerol-water

mixtures is included. Simulation results for high viscosity fluids are likewise presented with an emphasis on contrasting neck thinning dynamics as obtained from theory as well as experiments. Apart from contrasting neck shape and neck thinning dynamics, we also compare the break-up length and break-up time for glycerol-water mixtures using numerical simulations as well as experiments. The results included here utilize the VOF method implemented using FLOW-3D on a laptop computer, and as the simulations included here are carried out for axisymmetric flow, the implementation is carried out on a section, rather than 3D flow. We show that the VOF method provides accurate and robust results for drop formation and drop detachment of Newtonian fluids that compare very well with experimental visualization and analysis of dripping phenomena.

II. EXPERIMENTAL METHOD AND THE NUMERICAL APPROACH

A. Experiments

The experimental setup, as shown schematically in Fig. 1(a), includes a dispensing system that consists of a nozzle connected to a syringe pump and an imaging system that consists of a light source with a diffuser and a high-speed camera (Fastcam SA3) with a train of lenses [Nikkor 3.1 × zoom (18–25 mm) lens, plus a macro-lens] attached. The experimental method relies on the creation of a droplet by dripping, and the use of high speed imaging for obtaining images with high magnification, and at a high frame rate [up to 8000 fps (frames per second)]. The visualization and analysis of the columnar, neck region that undergoes capillary-driven thinning and pinch-off is used for measuring the neck radius as a function of time and for contrasting the pinch-off dynamics against theoretically obtained scaling laws and computational results. The minimum value of a liquid diameter that can be resolved with the setup used is 10 μm, and the resolution limit is set by the choice of the imaging system used in the experiments. The experimental videos of a drop formation process were analyzed using ImageJ[45] and MATLAB using specially written codes for edge detection and for determination of a minimum neck radius as a function of time.[24–27]

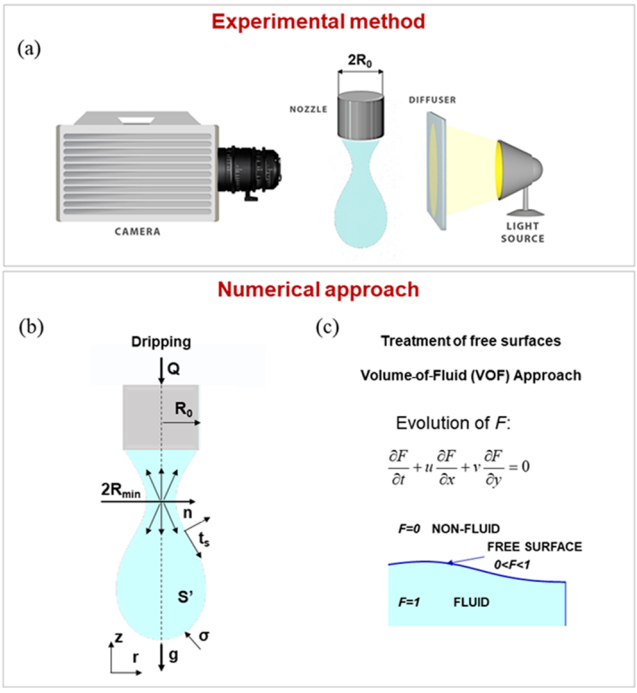

FIG. 1. Formation of a droplet from a capillary tube—problem description and volume-of-fluid (VOF) method. (a) The experimental setup consists of a high-speed camera, a light source, and a dispensing system. (b) A numerical simulation of drop formation from a cylindrical nozzle at a constant flow rate is performed. (c) Graphical representation of the VOF approach. The VOF method utilizes a scheme for locating and tracking a free surface introduced on the Eulerian-based fixed mesh.

B. Governing equations

The flow of incompressible Newtonian fluids of constant density, viscosity, and surface tension is investigated in a flow geometry corresponding to dripping, as shown in Fig. 1(b), using the VOF method embedded in FLOW-3D. The physical problem under investigation here involves an axisymmetric flow about the axis of symmetry, S'. Flow is modeled to be isothermal and incompressible. The incompressibility condition and equation of motion are given as

$$\nabla \cdot u = 0, \tag{1}$$

$$\rho\left(\frac{\partial \boldsymbol{u}}{\partial t} + \boldsymbol{u} \cdot \nabla \boldsymbol{u}\right) = \nabla \cdot \mathbf{T} + \mathbf{F}_b. \tag{2}$$

Here $\boldsymbol{u}$, $\mathbf{F}_b$, and $\mathbf{T}$ represent the velocity vector, the body force, and the Cauchy stress tensor, respectively. The Cauchy stress tensor is defined as $\mathbf{T} = -p\mathbf{I} + \boldsymbol{\tau}$, where p represents the isotropic pressure, $\mathbf{I}$ is the unit tensor, and $\boldsymbol{\tau}$ is the deviatoric stress tensor. For the incompressible Newtonian fluids, the deviatoric stress tensor exhibits a linear relation to the velocity gradient, $\boldsymbol{\tau} = \eta\left[\nabla u + (\nabla u)^{\mathrm{T}}\right]$, and thus follows Newton's law of viscosity. The boundary condition at the free surface is given as

$$\boldsymbol{n} \cdot \mathbf{T} = (2H\sigma)\boldsymbol{n}. \tag{3}$$

Here, σ represents the surface tension, $\boldsymbol{n}$ is a unit normal vector, and H is the mean Gaussian curvature of the free surface.

The implementation of VOF in FLOW-3D is based on the early work by Nichols and Hirt[40,41] that adapts an earlier numerical scheme for tracking a free surface called Marker-and-Cell (MAC) method.[46] The MAC method identifies and considers the grid cells that contain markers as occupied by fluid. Likewise, the cells without markers are called empty or void cells, whereas the cells that contain marker particles and have at least one neighboring grid cell that is empty are considered to be cells within which a free surface exists. Marker particles also define the location of fluid within a boundary cell. The MAC method for defining free surfaces requires

significantly higher computational storage and longer times for moving particles to new locations in contrast to the VOF method, as was pointed out by Hirt and Nichols.[40] Instead of using several points to the define regions occupied with fluid within a cell, the VOF method relies on using only one value for each dependent variable that defines the fluid within each cell in a mesh. The occupancy of the cells in the numerical grid is parameterized using a function F that has a value of unity in regions occupied by fluid and zero in regions without any fluid present [see Fig. 1(c)]. Cells that contain a free surface have a value of F between zero and one. The normal direction to the boundary corresponds to the direction in which the function F experiences the most rapid change. Since the VOF method consists of a scheme for locating and tracking a free surface introduced on the Eulerian-based fixed mesh, the evolution of the F field requires an algorithm. The following governing equation describes the time-dependent evolution of F:

$$\frac{\partial F}{\partial t} + u\frac{\partial F}{\partial x} + v\frac{\partial F}{\partial y} = 0. \tag{4}$$

The procedure for advancing a numerical solution in time with an increment δt consists of three steps outlined by Hirt and Nichols[40] for the VOF method described here. First, an explicit approximation for the equation of motion is used to compute the first guess for velocities, by using the initial conditions or previous time-level values for pressure, advection, and viscous accelerations. In the second step, pressure is adjusted in each cell in an iterative way to satisfy the continuity equation. In the final step, the function F is updated using a donor-acceptor flux approximation.[47]

C. The VOF method as implemented in *FLOW-3D*

Simulations of drop formation from a nozzle and those of liquid bridge break-up were performed using a uniform mesh size on an Asus laptop computer (with Intel® Core™ i7 4700HQ processor, Intel HM87 Express Chipset with memory: DDR3L 1600 MHz SDRAM up to 32 GB). The chosen mesh size for the simulations presented here is 0.007 cm such that the ratio of the cell length to the nozzle radius is approximately equal to 0.02. Only for the calculation of the total break-up length, the final droplet length was determined using the mesh size of 0.005 cm for a smaller mesh size helps in resolving smaller features before the pinch-off event. In such cases, the simulations were initiated using a mesh size of 0.007 cm, the smaller mesh size of 0.005 cm was implemented near the pinch-off event, and a dynamic change in the mesh was implemented to increase accuracy with a dramatic increase in the computational time. The ratio of the finest mesh cell (0.005 cm) to the nozzle radius was equal to 0.016. However, the reduction in the mesh size from 0.007 cm to 0.005 cm increases the computational time by approximately a factor of 10, while the differences observed in the overall shape of liquid neck shape, velocity profiles, and the radius evolution data obtained using these two different mesh sizes are relatively minor. Therefore, the larger mesh size (0.007 cm) was used for the simulations presented in this study, expect for the figure that required resolution of smaller features (for calculating the total break-up length).

In *FLOW-3D*, the built-in models for "Surface Tension" and "Gravity and non-inertial reference frame" were utilized for performing the numerical simulations. To compute the net surface tension force acting on each cell on the surface, the cells are viewed as control volumes for which surface tension stresses acting at cell sides are calculated. In this model, it is assumed that the equivalent surface pressure can replace surface tension forces. The surface tension model is sensitive to existing irregularities in the mesh due to its dependence on the curvature. Therefore, cubical control volumes are preferred. In the current study, a value of $\frac{R_i}{R_0} \approx 0.94$ was used for the low viscosity fluids listed in Table I and $\frac{R_i}{R_0} \approx 0.88$ was used for viscous fluids listed in Table II. Here R_i and R_0 represent the inner radius and outer radius of the nozzle, respectively. The chosen nozzle wall thickness is quite small in all cases, and the influence of wall thickness on the limiting drop length and the primary drop volume can be neglected according to Wilkes *et al.*,[37] provided that $\frac{R_i}{R_0} > 0.3$. The outer radius of the nozzle R_0 was used for non-dimensionalization in the study and assumed that fluid wets the nozzle perimeter during the drop formation process.

The fluid was dripped from the nozzle at a constant flow rate, Q = 1 ml/min. For the analysis presented in this manuscript, the first drop formed during each simulation was discarded and the dynamics of the second drop was analyzed. Analysis of the dynamics of the second drop aids in avoiding any influence of non-physical or transient behavior that could arise from the sudden start of the flow at the beginning of each simulation as discussed by Ambravaneswaran *et al.*[36] In certain cases, the dynamics of the second drop were compared to the dynamics of the subsequent third drop, and in all the cases presented herein, the dynamics were found to be quite similar.

TABLE I. Physical properties of simulated glycerol + water mixtures using *FLOW-3D*.

Fluid property	Fluid 1	Fluid 2	Fluid 3	Fluid 4	Fluid 5	Fluid 6	Fluid 7	Fluid 8
Glycerol concentration, ω (wt. %)	0	20	50	60	70	80	90	100
Viscosity, η (mPa s)	0.89	1.74	6	10.9	23.1	60.8	223.8	1413.8
Surface tension, σ (mN/m)	72.9	70.9	68	67.6	66.45	65.3	63.5	62.3
Density, ρ (g/cm^3)	0.998	1.047	1.126	1.153	1.181	1.207	1.235	1.261
Nozzle outer/inner diameter, D_0/D_i (mm)	3.2/3	3.2/3	3.2/3	3.2/3	3.2/3	3.2/3	3.2/3	3.2/3
Ohnesorge number, Oh	0.003	0.005	0.017	0.031	0.065	0.17	0.63	3.99

TABLE II. Physical properties of simulated high viscosity fluids using *FLOW-3D*.

Fluid property	Fluid 9	Fluid 10	Fluid 11	Fluid 12	Fluid 13
Viscosity, η (Pa · s)	2.0	1.5	0.8	0.4	0.25
Surface tension, σ (mN/m)	68	68	68	68	68
Density, ρ (g/cm^3)	1.0	1.0	1.0	1.0	1.0
Nozzle outer/inner radius, R_0/R_i (mm)	1.7/1.5	1.7/1.5	1.7/1.5	1.7/1.5	1.7/1.5
Ohnesorge number, Oh	8.32	6.24	3.33	2.08	1.04

Surface tension driven pinch-off of a newly formed drop, also denoted as a singular point, occurs after the gravitational force overcomes the surface tension force ($mg > 2\pi\sigma R_0$, where m represent the mass of a drop).

III. RESULTS AND DISCUSSION

A. Neck shape and filament radius evolution of low viscosity fluids

Drop formation and its detachment from the bulk fluid accumulated at the stainless-steel nozzle tip are simulated using the VOF method implemented in FLOW-3D, first for fluids with low viscosity and physical properties listed in Table I. In the snapshots of simulated fluid neck evolution shown in Fig. 2 for two low-viscosity fluids (water and 50 wt. % glycerol in water mixture), the formation of satellite drops is clearly captured and visualized. By contrast, although previous studies by Zhang[42] and Gueyffier *et al.*[44] successfully computed the drop profile during the thinning and break-up process, the resolution of their VOF calculations was not sufficiently high to capture the satellite drop formation.[48]

Chen and Steen[49] were the first to examine angles made with the z-axis by the two conical menisci that meet at a point of the pinch-off, and later Day *et al.*[50] used potential flow arguments, to derive the cone angle as well as the inertio-capillary scaling expression,

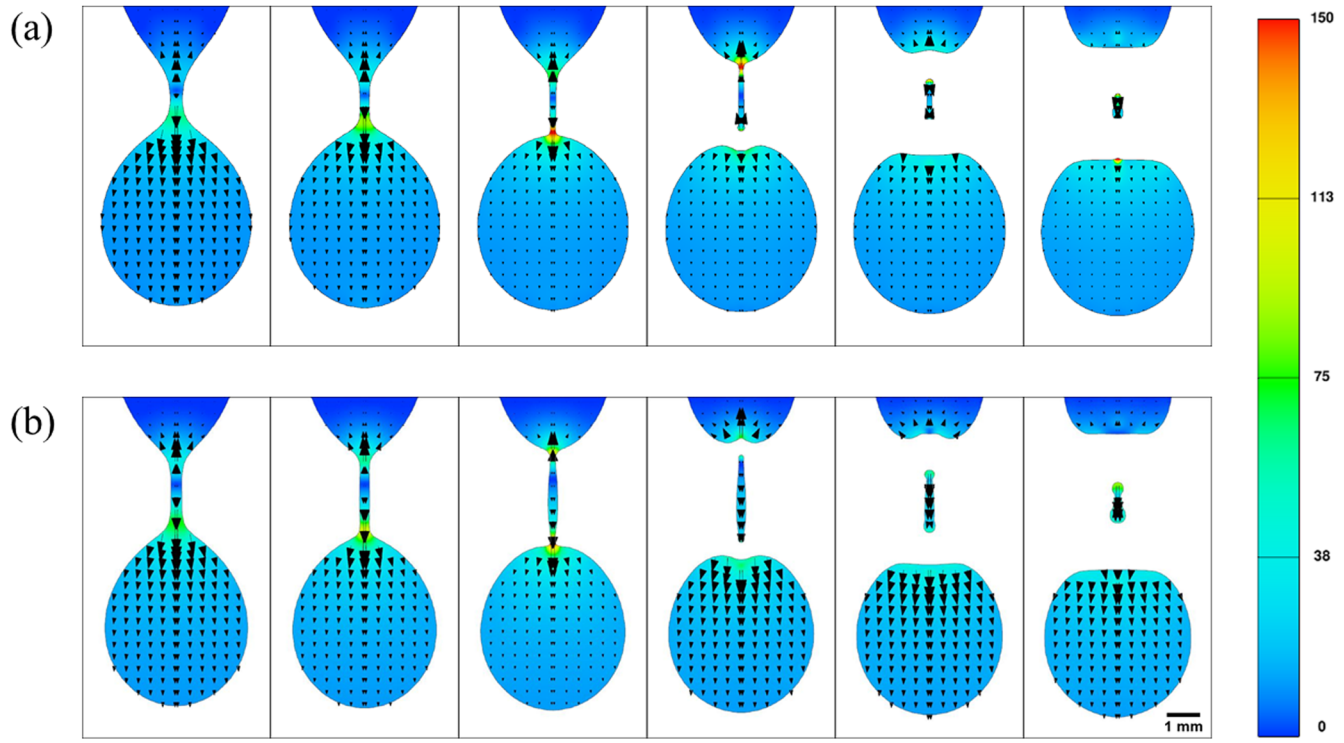

FIG. 2. Sequence of images showing capillary-driven neck evolution and droplet formation for low-viscosity fluids. (a) A sequence of simulated images of water (0 wt. % glycerol) shows neck formation and subsequent thinning and pinch-off dynamics including the formation of the satellite drop. (b) A sequence of images shows neck radius evolution and drop detachment for the low viscosity fluid composed of 50 wt. % glycerol in water. The time step between images is 500 μs, and the scale bar represents a length of 1 mm for the two cases shown. The color bar shows the velocity field in units of cm/s. The addition of glycerol seems to exercise a relatively minor influence on pinch-off dynamics despite a five-fold increase in viscosity.

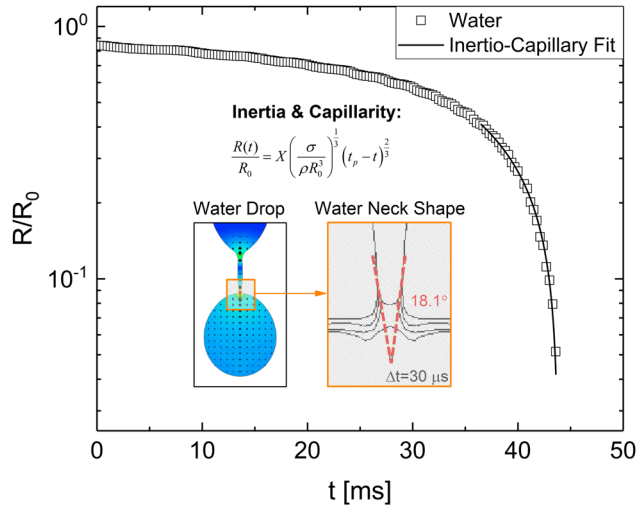

FIG. 3. Computed evolution of the minimum radius of the water neck during the drop formation and detachment process. The instantaneous neck radius of water and the inertio-capillary fit are shown. The inset shows a self-similar nature of neck thinning dynamics close to a pinch-off moment. The characteristic cone angle of 18.1° as predicted by Day *et al.*[50] and visualized in experiments[52] is captured well using the VOF method.

$$\frac{R(t)}{R_0} = X\left(\frac{\sigma}{\rho R_0^3}\right)^{\frac{1}{3}}(t_p - t)^{\frac{2}{3}}. \quad (5)$$

Figure 3 shows computed time-dependent radius evolution of a water neck with an inertio-capillary fit (black solid line). The characteristic exponent value of 2/3 as anticipated from the theory and also observed in previous experiments[3,4,24–27,33,49–52] describes the dynamics close to the pinch-off. According to the asymptotic theoretical expression [Eq. (5)], the pinch-off dynamics of inviscid fluids are unaffected by changes in fluid viscosity, and the characteristic inertio-capillary time scale, also known as Rayleigh time $t_R = \left(\rho R_0^3/\sigma\right)^{1/2}$, depends only on the density and surface tension of the fluids. The X in Eq. (5) represents a numerical pre-factor previously found to be X = 0.6-0.8.[53] Fluids 1-5 in Table I (i.e., for glycerol concentration of and below 70 wt. %) can be classified as low viscosity fluids, i.e., $Oh < 0.1$, and based on theory, are expected to show inertio-capillary thinning behavior.

The image sequences obtained from dripping experiments shown in Fig. 4(a) compared well with the results obtained from the numerical simulations [using the VOF method as implemented in FLOW-3D and shown in Fig. 4(b)] for a representative glycerol-water mixture containing 70 wt. % glycerol. In Figs. 4(c) and 4(d), the instantaneous filament radius rescaled with a nozzle radius, R/R_0, is plotted as a function of shifted time, $t_p - t$, on a log-log scale to highlight the power law dependent scaling near pinch-off (approach from the right to left). Lines of the best fit (dashed lines) included in the figure for the simulated data exhibit the slope of 2/3, in agreement with inertio-capillary scaling [see Eq. (5), shown as bold black dashed line]. The datasets appear to lie close together since the absolute volute of vertical shift depends on the variation in density and surface tension, and in a log-log plot, the overall shift is relatively small for this range of glycerol concentrations.

In Fig. 4(c), four datasets obtained by capturing neck thinning dynamics in dripping experiments for glycerol-water mixtures (with 0, 20, 50, and 70 wt. % glycerol) are shown,

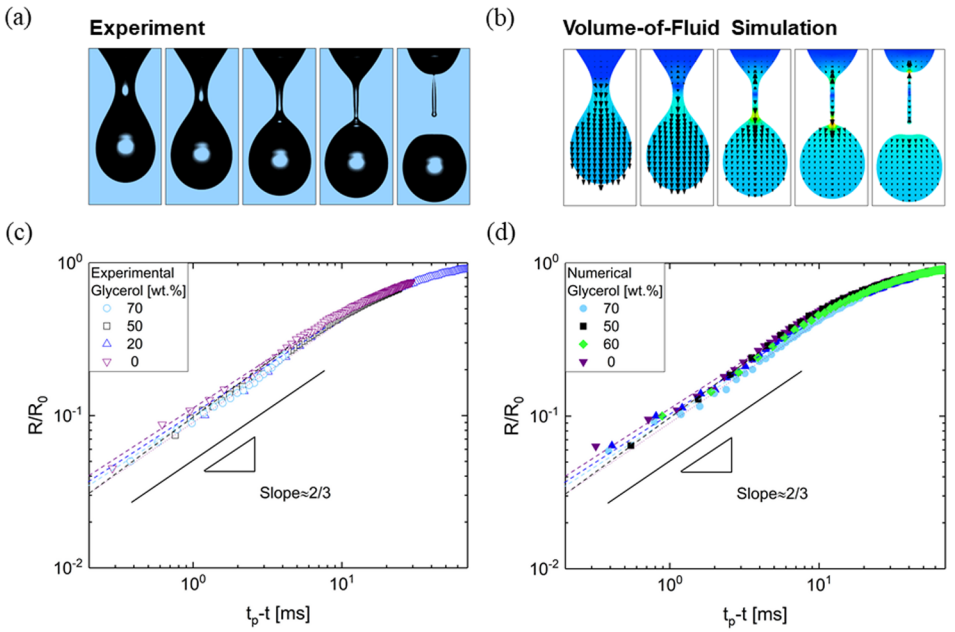

FIG. 4. Comparison of experiments and simulations depicting drop formation for low viscosity glycerol/water mixtures. [(a) and (b)] The image sequences obtained from (a) experiments and (b) simulations (in color online) show good agreement. The simulated drop profiles shown in (b) are colored by the velocity magnitude [in the range of 0 (dark blue) to 130 cm/s (red)], and velocity vectors are shown in the images. [(c) and (d)] Radius evolution in time of the liquid filament formed during the drop formation process for both (c) experimental and (d) numerical results is presented. A characteristic slope of 2/3, anticipated for radius evolution near pinch-off of low viscosity fluids, is in agreement with simulated profiles.

while datasets shown in Fig. 4(d) represent radius evolution profiles of simulated drop formation processes using FLOW-3D. A close comparison of datasets shown in Figs. 4(c) and 4(d) reveals an excellent agreement between radius evolution data obtained from numerical simulations and experiments. The numerical pre-factor X included in the equation was determined by Chen *et al.*[54] using a numerical simulation to be close to 0.7 (we find X = 0.64 using the data including Fig. 3 in the work of Chen *et al.*[54]), and it became the value commonly used in place of X in Eq. (5),[4,22,55–57] with some experimentalist reporting 0.8 as a prefactor.[22,58,59] However, we find that the value determined by fitting the radius evolution datasets obtained from both VOF simulations and experiments is close to X = 0.4 although on mining through all our present and previously reported experiments,[24–27] we find that the value predicted by the analysis of Chen and co-workers[54] is approached asymptotically in only a few experiments if neck radius evolution is analyzed to a lower resolution (down to a micron) than achieved here.

B. Dripping of higher viscosity fluids: Thinning dynamics and break-up length

For innumerable dispensing applications that require liquid transfer from a nozzle to a substrate, evaluating the break-up length is as important as capillary-driven thinning and pinch-off dynamics that determine the break-up time. Since stream-wise velocity gradients associated with extensional flow field arise within the columnar necks undergoing capillary-driven thinning during dripping, radius evolution can be analyzed for characterizing extensional rheology response and printability.[22,53,58] However, if the camera is kept fixed, the length of the neck before break-up presents a practical difficulty in obtaining thinning dynamics with high resolution. Therefore, we compare and contrast the break-up length of glycerol-water mixtures with fluid properties listed in Table I. A pronounced increase in the break-up length and break-up time is observed only after the glycerol content is increased beyond 70 wt. %, as illustrated in Fig. 5. In the sequence of snapshots of the simulated drop profiles for glycerol (100 wt. %, no water added) with a time step of 5 ms shown in Fig. 5(a), the neck profile is long and slender. The neck shape, time scale of evolution, and break-up length are quite distinct from the profiles obtained for water and low viscosity fluids (see Figs. 2–4). Neck shapes before pinch-off shown in Fig. 5(b) for three glycerol-water mixtures illustrate the dramatic shift in neck thinning dynamics and break-up length due to an increase in viscosity. The simulated break-up length values show trends in close agreement with the experimental and numerical simulation results.

Scaled break-up length computed using the VOF approach for the entire range of glycerol-water mixtures is compared with the experimental data collected as a part of this study in Fig. 6. The FEM-based computation results from Wilkes *et al.*[37] are also included. The VOF and FEM numerical

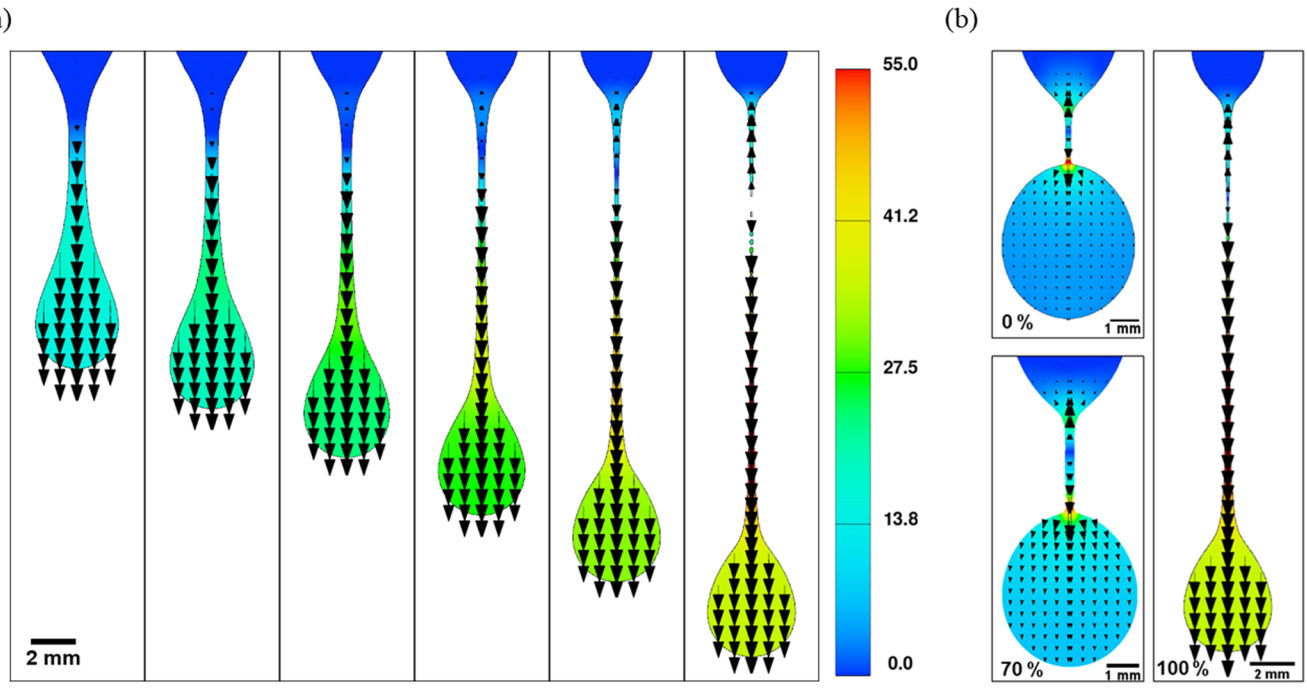

FIG. 5. Glycerol thinning image sequence and break-up length visualization for three cases. (a) Glycerol thinning is shown through a sequence of snapshots with a time step Δt = 5 ms and reveals quite different dynamics compared to previously seen for low viscosity fluids. The length of a filament changes significantly when the glycerol content increases above 70 wt. %. (b) Final lengths of the simulated liquid filaments before pinch-off for three cases of glycerol + water mixtures (0 wt. %, 70 wt. %, and 100 wt. %).

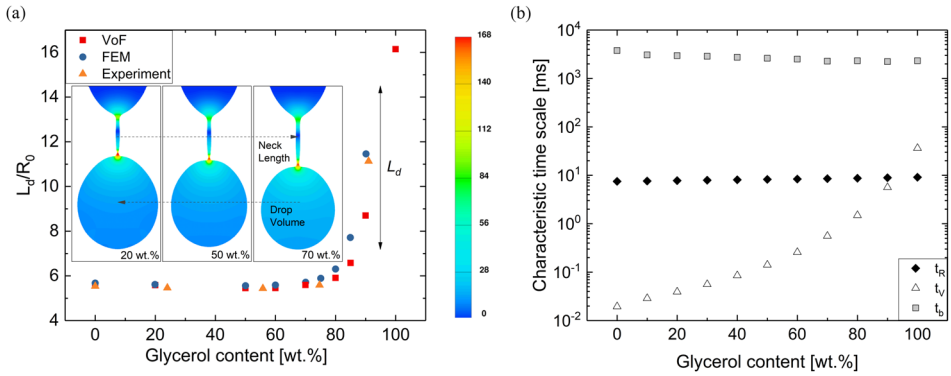

FIG. 6. Length of a drop before pinch-off for water-glycerol mixtures and characteristic time scales. (a) Computed values of the drop length in the frame leading to pinch-off are plotted against glycerol mass concentration and compared to dataset provided by Wilkes *et al.*[37] Drop length consists of a freshly formed drop and the rest of the fluid at the bulk around the nozzle tip. The inset shows drop profiles before a point of break-up for three mass concentrations of glycerol. The three images shown in the inset represent the last captured frames leading to pinch-off for three different contents of glycerol in the glycerol + water mixture. The drop profiles are colored by the velocity magnitude (in units of cm/s). (b) Three characteristic time scales (Rayleigh or inertio-capillary time, t_R; viscocapillary time, t_v; and break-up time, t_b = pinch-off time, t_p) are shown as a function of glycerol concentration.

simulations, as well as experiments, show that inviscid fluids (glycerol content < 70 wt. %) exhibit inertio-capillary thinning ($Oh < 0.1$), and the break-up length appears to show a very little change for these solutions. On a careful examination of both experimental and simulated datasets for inviscid fluids (glycerol content < 70 wt. %), it can be seen that the break-up length decreases modestly with an increase in the glycerol content from 0 wt. % to 50 wt. % and increases beyond 50 wt. %. The minimum can be explained by recalling that though viscosity and density increase as the mass fraction of glycerol in the mixture is increased, the value of surface tension decreases. The inset in Fig. 6(a) shows the drop profiles for three concentrations of glycerol in the mixture. Even though the neck shapes in Fig. 6(a) appear conical for all three drops displayed in the inset, the angle of 18.1° is not recovered in all three cases. Similar conclusions were drawn by Wilkes *et al.*[37] for their FEM results showed that the cone angle decreases as the mass concentration of glycerol increases.

In contrast to inviscid fluids where radius evolution follows inertio-capillary thinning before pinch-off and where the characteristic time scale (Rayleigh time) is set only by density and surface tension, the break-up length and break-up time for glycerol-rich solutions (c > 70 wt. %) show a strong concentration-dependent increase, as shown in Fig. 6(a). We will show later that the capillary-driven thinning and pinch-off dynamics of these mixtures display the viscocapillary thinning scaling,

$$\frac{R}{R_o} = 0.0709\frac{\sigma}{\eta R_0}(t_p - t) = 0.0709\left(\frac{t_p - t}{t_v}\right). \quad (6)$$

The linear relationship between the neck radius and time to pinch-off was derived by Papageorgiou,[60] and although Eggers[3,33] derived an expression with a different prefactor, Tripathi and McKinley[61] showed that Papageorgiou's scaling expression captures the experimental data for glycerol-water mixtures. Papageorgiou[60] obtained the similarity solution using a slender cylinder approximation for a viscous liquid column. In the viscocapillary (VC) scaling, t_v represents the characteristic viscocapillary time scale. The viscocapillary time $t_v = t_R\,Oh$ depends on both the Ohnesorge number Oh and Rayleigh time t_R and increases with viscosity. Although the break-up length obtained from numerical simulations shows excellent agreement with the FEM simulations and our experiments with low viscosity fluids, for higher viscosity cases (with $Oh > 0.2$), a slight discrepancy arises which can be attributed to iterated stretching. Shi *et al.*[32] experimentally observed that dripping of a highly viscous liquid results in iterated stretching, such that each subsequent neck being thinner than the previous one. Even though a finer mesh could potentially result in bringing simulations into closer agreement with theory, we chose to not pursue those computationally intensive calculations since we verified that the simulated neck thinning dynamics closely emulate experimental results up to the neck radius of 10 μm.

The break-up time as a function of glycerol fraction is contrasted with the Rayleigh time and viscocapillary time in Fig. 6(b). Although viscocapillary time shows an increase of several orders of magnitude across the concentration range, both the Rayleigh time and break-up time appear to have only a modest concentration dependence. The Rayleigh time shows a mild increase with an increase in the glycerol content, while the break-up time shows a modest decrease. Although Wilkes *et al.*[37] also pointed the minima at 50 wt. % glycerol and a large increase in the break-up length above 70 wt. %, the comparison of characteristic time scales against the break-up time was not previously made. The significant and highly nonlinear change in the overall break-up length above 70 wt. % glycerol can be correlated with the concentration-dependent increase in the viscosity of glycerol-water mixtures. Even though viscosity changes by three orders of magnitude between pure water and pure glycerol, the bulk of this enhancement in

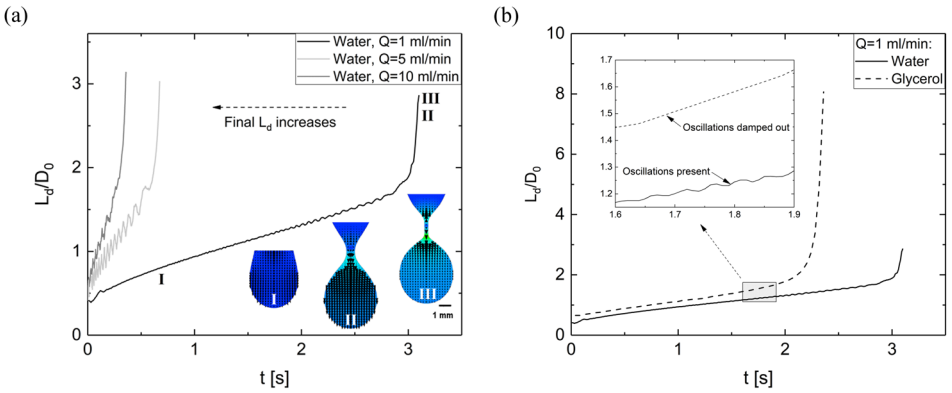

FIG. 7. Variation of the length of the droplet during the water drop formation process for three different flow rates and a comparison of drop evolution processes for water and glycerol. (a) The increase in the flow rate causes fluid to experience a faster approach to the break-up moment and results in longer total droplet lengths before a pinch-off moment. (b) A comparison of droplet length evolution during drop formation for water and glycerol. The inset shows oscillations of the water droplet present during drop formation that causes the dynamics of water droplet formation to become slower.

viscosity occurs above 70 wt. % glycerol and the viscosity of 70 wt. % glycerol is only an order of magnitude higher than that of pure water. Since the surface tension interpolates between 60 and 72 mN/m, the value of dimensionless viscosity or Oh is dictated primarily by the change in shear viscosity, and for low viscosity ($Oh < 0.1$) fluids, inertio-capillary thinning governs the pinch-off dynamics.

The effect of increase in the volume flow rate on the total droplet length during a drop formation process is shown in Fig. 7(a). A lower flow rate allows a newly formed droplet to spend more time exploring shapes similar to that of a section of a sphere, thus resulting in significantly longer break-up times, even though the dynamics before pinch-off display analogous inertio-capillary behavior. As a drop emerges from a nozzle tip, the interplay of capillarity and gravity that are of comparable magnitude determines the shape as shown for water in stage I in Fig. 7(a). Due to the sustained increase in droplet mass, gravity eventually overwhelms capillarity. Consequently, an accelerated increase in the length of a droplet is observed, and simultaneously, the neck undergoes rapid thinning, culminating in pinch-off [see droplet shapes denoted as II and III in Fig. 7(a)]. Visualization of the velocity field for three simulated shapes of the droplets shown in Fig. 7(a) reveals that the flow field during the droplet formation process becomes purely extensional only close to pinch-off as seen in the image of a simulated droplet denoted as III. The comparison of droplet formation for two fluids with a large difference in viscosity values (water and glycerol) at a fixed flow rate (Q = 1 ml/min) shown in Fig. 7(b) reiterates the conclusions drawn from the analysis of break-up length and break-up time. A close examination of data reveals that the formation of a water droplet (solid line) takes approximately 1.3× longer time compared to a highly viscous glycerol droplet (dashed line) due to oscillations that occur while the drop is evolving and before gravity overcomes capillarity. The oscillations are more pronounced for lower viscosity fluids and thus affect the duration of the drop formation process, whereas the oscillations are damped out in higher viscosity fluids.

The effect of the increase in fluid viscosity on the neck shape and radius evolution obtained from VOF based numerical simulations is contrasted against experiments for 80 wt. % glycerol in water in Fig. 8. The neck shapes are slender and cylindrical in both experiments and numerical simulations as shown in Fig. 8(a). Likewise, the neck radius evolution data

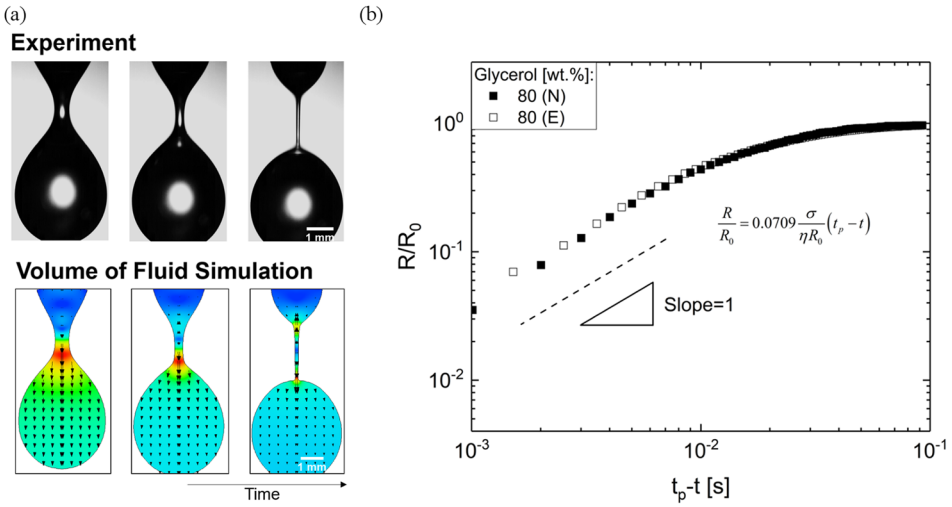

FIG. 8. Comparison of experiments and simulations for the case of a drop formation for 80 wt. % glycerol and water mixture. (a) A set of images obtained from experiments (upper row) and simulations (bottom row) with a time step of 1 ms show good agreement. The simulated drop profiles shown in the bottom row are colored by the velocity magnitude [ranging from 0 (dark blue) to 100 cm/s (red) and colored online], and velocity vectors are shown in the images. (b) Radius evolution with time of liquid filament formed during the drop formation process is shown on a log-log plot for the two cases.

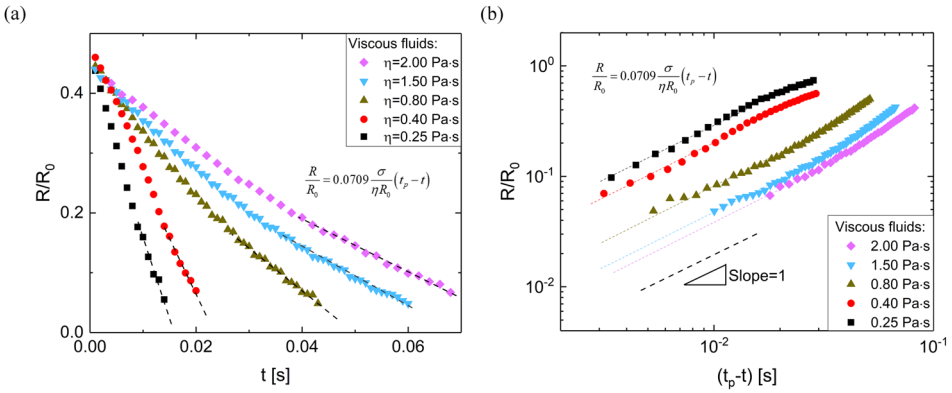

FIG. 9. Viscocapillary thinning and pinch-off of viscous Newtonian fluids. (a) Linear-linear plot captures thinning dynamics of viscous filaments revealing that thinning becomes linear with time when a pinch-off moment is approached in simulations of drop formation and (b) numerically computed radius evolution of a filament with time for a set of viscous fluids is shown on a log-log plot. In all five cases, the filament thinning dynamics become linear toward the pinch-off. The lines of best fit are shown as well as line showing the slope of 1.

obtained from the numerical simulations match closely with the experimental data, as shown in Fig. 8(b). Here the dimensionless minimum neck radius plotted against the time interval from pinch-off instant on a log-log axis such that pinch-off is approached from the right to left follows the viscocapillary scaling quite well.

In order to further investigate the possibility of using the VOF method as implemented in FLOW-3D to simulate pinch-off dynamics of highly viscous fluids with a viscosity of $250\eta_{water}$ and above, numerical simulations were carried out with fluid properties listed in Table II. The properties were chosen such that the surface tension and density of fluids are kept fixed, implying that the Rayleigh time for all the fluids is kept constant, while the Oh number of these fluids increases in proportion to the change in viscosity. Since the viscocapillary time $t_v = t_R\,Oh$ depends on both the Ohnesorge number Oh and Rayleigh time t_R, here the viscocapillary time decreases from fluids 9 to 13 in proportion to the corresponding decrease in viscosity of the fluid. The neck thinning dynamics for these viscous fluids determined using the VOF method based numerical simulation of dripping are shown in Fig. 9. In Fig. 9(a), the radius evolution datasets are presented on a linear-linear plot against time with the purpose of highlighting the effect of increasing viscous contribution (and viscocapillary time). Due to our choice of parameters, the decrease in the slope and increase in pinch-off time are both directly correlated with the corresponding increase in viscosity.

Furthermore, in Fig. 9(a), the radius evolution data before the pinch-off instant t_p can be seen to follow the viscocapillary thinning behavior, and here the dashed lines represent corresponding fits to the neck radius extracted from numerical simulations of dripping carried out using FLOW-3D. The radius evolution profiles R/R_0 (here $R_0 = 0.85$ mm) are additionally shown as a function of shifted time $(t_p - t)$ on a log-log plot. As the pinch-off is approached (again, the thinning proceeds from the right to left), lines of the best fit for each dataset included (dashed lines) display the linear dependence expected from viscocapillary scaling. Thus, the VOF method implemented in FLOW-3D captures dripping behavior of highly viscous fluids quite well, for viscosity values up to three orders of magnitude higher than previous unsuccessful studies.

IV. CONCLUSIONS

We show that the VOF technique (implemented in FLOW-3D) allows accurate and reliable determination of pinch-off dynamics of Newtonian fluids, and we benchmark the numerical results against experimental studies, included herein. We show that the self-similar neck evolution obtained from the computational analysis using the VOF approach can be described by the scaling laws obtained from theoretical, experimental, and numerical analysis. We find that the simulated radius evolution profiles match the scaling laws and pinch-off dynamics that are experimentally observed and theoretically predicted for low viscosity fluids (with $Oh < 0.1$, classified as inviscid fluids). The computational analysis shows that the neck profile for low viscosity Newtonian fluids becomes self-similar and conical, with a cone angle of 18.1° in agreement with theory,[50,51] close to the pinch-off instant. Rich dynamics before and after the pinch-off event including the formation of a conical neck, surface overturning, and the formation of satellite drops are all captured in these simulations. For fluids with relatively high viscosities, our results indicate that the thinning dynamics are captured by viscocapillary scaling, quantitatively agreeing with the experiments. We are able to simulate the neck shape and neck thinning dynamics as well as satellite drop formation quite accurately for viscosity values up to three orders of magnitude greater than the viscosity values said to be untenable based on earlier studies. The rationale for testing low viscosity fluids is due to their common use in various applications such as inkjet printing in which the typical viscosity value of utilized printing inks is lower than 15 mPa · s. On the other hand, high fluid viscosities are desirable in food or cosmetic dispensing applications or in applications involving printing of various three-dimensional structures.

While the break-up length of low viscosity fluids is quite insensitive to increase in viscosity, for $Oh > 0.1$, the break-up length increases dramatically with an increase in fluid viscosity. The observations are quite pertinent to the design of

dripping-based experiments for extensional viscosity characterization. Even though the iterated stretching of high viscosity fluids observed in highly stretched, long cylindrical slender necks is not simulated for the chosen mesh size in simulations presented here, the neck radius data included herewith from simulations match the experimentally observed radius evolution quite nicely. The simulations also reveal that the overall break-up time during dripping at a constant flow rate can be much longer for the low viscosity fluids that follow inertio-capillary thinning in pinch-off as the oscillations dominate the early evolution of emerging and growing drop, in comparison with highly viscous drops, where oscillations are damped out and final thinning displays viscocapillary behavior.

Stream-wise velocity gradients associated with extensional flow field arise within the columnar necks undergoing capillary-driven thinning. The VOF method implemented in FLOW-3D allows a robust evaluation of the magnitude of the underlying stresses and extensional flow field (both uniformity and magnitude). The visualization of the flow field within the thinning liquid filament shows that the flows become truly extensional only when the neck radius shape reaches its final self-similar shape. In rheologically complex fluids, extra elastic stresses, as well as non-Newtonian shear and extensional viscosity, dramatically alter the nonlinear pinch-off dynamics.[4,11,24,27] The present study represents a sensible step toward performing a rigorous computational analysis of the nonlinear dynamics critical for finite-time singularity of non-Newtonian fluids, as well as processability and printability in more complex geometries. The benchmarking studies presented herein are necessary first steps toward developing algorithms and modules implemented using the VOF technique to evaluate free surface flows in the presence of additional complexity that could arise due to any one of the following: moving contact lines, non-axisymmetric flows, interfacial rheology, evaporative losses, Marangoni effects, and for complex fluids, the effect of non-Newtonian viscosity, extensional rheology response, and normal stresses. Furthermore, experimental protocols used in Capillary Break-up Extensional Rheometer (CaBER),[4,57] Rayleigh-Ohnesorge Jetting Extensional Rheometer (ROJER),[11,15,38,62,63] Dripping-onto-Substrate (DoS) Rheometry,[24–27,64–66] and several others[19,20,58,67–71] rely on the visualization and analysis of neck thinning dynamics in prototypical geometries for characterizing material properties that determine jettability, printability, spinnability, and sprayability of simple and complex fluids. The analysis of free surface flows of complex fluids in various geometries using FLOW-3D remains a part of the future studies. Graphic inks conventionally used in ink-jet printing are low viscosity fluids, with low particle loading, that exhibit rate-independent shear viscosity and limited or no viscoelasticity. In contrast, unconventional inks containing DNA, cells, or proteins,[72–74] high-particle loading suspensions, photovoltaic or inorganic materials like fullerene or graphene,[75] can exhibit higher, and rate-dependent, shear viscosity, and highly nonlinear viscoelastic response. Emphasis on additive manufacturing through rapid, precise deposition of such unconventional inks has created additional need for understanding and characterizing free surface flows. However, progress in both computational methods and easier availability of computational resources present the possibility that in the future, computational fluid dynamics will be used increasingly and most frequently by engineers, designers, formulators, scientists, and students or scientists in academia.

ACKNOWLEDGMENTS

The paper is dedicated to Professor Robert Bird on his 95th birthday. The authors wish to acknowledge the scientists and engineers at Flow Science for significant feedback and support. In particular, we would like to thank Amir Isfahani and Dan Milano for addressing our questions and for a close reading of the manuscript. V.S. would like to acknowledge funding support by the College of Engineering and the Department of Chemical Engineering at University of Illinois at Chicago. The student (J.D.) was supported by the start-up funds as well as teaching assistantship provided by the Department of Chemistry. The authors would like to thank Professor Cynthia Jameson and Professor Lewis Wedgewood, UIC, for a close reading of the manuscript.

REFERENCES

[1] H. A. Stone, "Dynamics of drop deformation and breakup in viscous fluids," Annu. Rev. Fluid Mech. **26**, 65 (1994).
[2] S. Middleman, *Modeling Axisymmetric Flows: Dynamics of Films, Jets and Drops* (Academic Press, San Diego, 1995).
[3] J. Eggers, "Nonlinear dynamics and breakup of free-surface flows," Rev. Mod. Phys. **69**, 865 (1997).
[4] G. H. McKinley, "Visco-elasto-capillary thinning and break-up of complex fluids," Rheol. Rev. **2005**, 1.
[5] B. Derby, "Inkjet printing of functional and structural materials: Fluid property requirements, feature stability, and resolution," Annu. Rev. Mater. Res. **40**, 395 (2010).
[6] N. Ashgriz, *Handbook of Atomization and Sprays: Theory and Applications* (Springer, New York, 2011).
[7] O. A. Basaran, H. Gao, and P. P. Bhat, "Nonstandard inkjets," Annu. Rev. Fluid Mech. **45**, 85 (2013).
[8] S. Kumar, "Liquid transfer in printing processes: Liquid bridges with moving contact lines," Annu. Rev. Fluid Mech. **47**, 67 (2014).
[9] O. A. Basaran, "Small-scale free surface flows with breakup: Drop formation and emerging applications," AlChE J. **48**, 1842 (2002).
[10] A. L. Yarin, *Free Liquid Jets and Films: Hydrodynamics and Rheology* (Longman Scientific and Technical, 1993).
[11] V. Sharma, S. J. Haward, J. Serdy, B. Keshavarz, A. Soderlund, P. Threlfall-Holmes, and G. H. McKinley, "The rheology of aqueous solutions of ethyl hydroxy-ethyl cellulose (EHEC) and its hydrophobically modified analogue (hmEHEC): Extensional flow response in capillary break-up, jetting (ROJER) and in a cross-slot extensional rheometer," Soft Matter **11**, 3251 (2015).
[12] J. Eggers and E. Villermaux, "Physics of liquid jets," Rep. Prog. Phys. **71**, 036601 (2008).
[13] R. H. Fernando, L. L. Xing, and J. E. Glass, "Rheology parameters controlling spray atomization and roll misting behavior of waterborne coatings," Prog. Org. Coat. **42**, 284 (2001).
[14] J. P. Rothstein, "Strong flows of viscoelastic wormlike micelle solutions," Rheol. Rev. **2008**, 1 (2001).
[15] B. Keshavarz, V. Sharma, E. C. Houze, M. R. Koerner, J. R. Moore, P. M. Cotts, P. Threlfall-Holmes, and G. H. McKinley, "Studying the effects

of elongational properties on atomization of weakly viscoelastic solutions using Rayleigh Ohnesorge jetting extensional rheometry (ROJER)," J. Non-Newtonian Fluid Mech. **222**, 171 (2015).
[16]A. R. Abate, J. Thiele, and D. A. Weitz, "One-step formation of multiple emulsions in microfluidics," Lab Chip **11**, 253 (2011).
[17]G. F. Christopher and S. L. Anna, "Microfluidic methods for generating continuous droplet streams," J. Phys. D: Appl. Phys. **40**, R319 (2007).
[18]P. Garstecki, M. J. Fuerstman, H. A. Stone, and G. M. Whitesides, "Formation of droplets and bubbles in a microfluidic T-junction–Scaling and mechanism of break-up," Lab Chip **6**, 437 (2006).
[19]M. Stelter, G. Brenn, A. L. Yarin, R. P. Singh, and F. Durst, "Validation and application of a novel elongational device for polymer solutions," J. Rheol. **44**, 595 (2000).
[20]Y. Christanti and L. M. Walker, "Effect of fluid relaxation time of dilute polymer solutions on jet breakup due to a forced disturbance," J. Rheol. **46**, 733 (2002).
[21]M. S. N. Oliveira and G. H. McKinley, "Iterated stretching and multiple beads-on-a-string phenomena in dilute solutions of highly extensible flexible polymers," Phys. Fluids **17**, 071704 (2005).
[22]V. Tirtaatmadja, G. H. McKinley, and J. J. Cooper-White, "Drop formation and breakup of low viscosity elastic fluids: Effects of molecular weight and concentration," Phys. Fluids **18**, 043101 (2006).
[23]C. Clasen, J. P. Plog, W. M. Kulicke, M. Owens, C. Macosko, L. E. Scriven, M. Verani, and G. H. McKinley, "How dilute are dilute solutions in extensional flows?," J. Rheol. **50**, 849 (2006).
[24]J. Dinic, Y. Zhang, L. N. Jimenez, and V. Sharma, "Extensional relaxation times of dilute, aqueous polymer solutions," ACS Macro Lett. **4**, 804 (2015).
[25]J. Dinic, M. Biagioli, and V. Sharma, "Pinch-off dynamics and extensional relaxation times of intrinsically semi-dilute polymer solutions characterized by dripping-onto-substrate rheometry," J. Polym. Sci., Part B: Polym. Phys. **55**, 1692 (2017).
[26]L. N. Jimenez, J. Dinic, N. Parsi, and V. Sharma, "Extensional relaxation time, pinch-off dynamics and printability of semi-dilute polyelectrolyte solutions," Macromolecules **51**, 5191 (2018).
[27]J. Dinic, L. N. Jimenez, and V. Sharma, "Pinch-off dynamics and dripping-onto-substrate (DoS) rheometry of complex fluids," Lab Chip **17**, 460 (2017).
[28]C. Clasen, P. M. Phillips, and L. Palangetic, "Dispensing of rheologically complex fluids: The map of misery," AIChE J. **58**, 3242 (2012).
[29]F. M. Huisman, S. R. Friedman, and P. Taborek, "Pinch-off dynamics in foams, emulsions and suspensions," Soft Matter **8**, 6767 (2012).
[30]M. Pasquali and L. E. Scriven, "Free surface flows of polymer solutions with models based on the conformation tensor," J. Non-Newtonian Fluid Mech. **108**, 363 (2002).
[31]R. Scardovelli and S. Zaleski, "Direct numerical simulation of free-surface and interfacial flow," Annu. Rev. Fluid Mech. **31**, 567 (1999).
[32]X. D. Shi, M. P. Brenner, and S. R. Nagel, "A cascade of structure in a drop falling from a faucet," Science **265**, 219 (1994).
[33]J. Eggers and M. A. Fontelos, *Singularities: Formation, Structure, and Propagation* (Cambridge University Press, Cambridge, UK, 2015).
[34]J. R. Lister and H. A. Stone, "Capillary breakup of a viscous thread surrounded by another viscous fluid," Phys. Fluids **10**, 2758 (1998).
[35]J. Eggers and T. F. Dupont, "Drop formation in a one-dimensional approximation of the Navier-Stokes equation," J. Fluid Mech. **262**, 205 (1994).
[36]B. Ambravaneswaran, E. D. Wilkes, and O. A. Basaran, "Drop formation from a capillary tube: Comparison of one-dimensional and two-dimensional analyses and occurrence of satellite drops," Phys. Fluids **14**, 2606 (2002).
[37]E. D. Wilkes, S. D. Phillips, and O. A. Basaran, "Computational and experimental analysis of dynamics of drop formation," Phys. Fluids **11**, 3577 (1999).
[38]A. Ardekani, V. Sharma, and G. H. McKinley, "Dynamics of bead formation, filament thinning and breakup of weakly viscoelastic jets," J. Fluid Mech. **665**, 46 (2010).
[39]H. Tronnolone and Y. M. Stokes, "Pinch-off masses of very viscous fluids extruded from dies of arbitrary shape," Phys. Fluids **30**, 073103 (2018).
[40]C. W. Hirt and B. D. Nichols, "Volume of fluid (VoF) method for the dynamics of free boundaries," J. Comput. Phys. **39**, 201 (1981).
[41]B. Nichols and C. Hirt, *Methods for Calculating Multi-dimensional, Transient, Free Surface Flows Past Bodies* (Naval Ship Research and Development Center, Bethesda, MD, 1975).
[42]X. G. Zhang, "Dynamics of growth and breakup of viscous pendant drops into air," J. Colloid Interface Sci. **212**, 107 (1999).
[43]V. R. Gopala and B. G. M. van Wachem, "Volume of fluid methods for immiscible-fluid and free-surface flows," Chem. Eng. J. **141**, 204 (2008).
[44]D. Gueyffier, J. Li, A. Nadim, R. Scardovelli, and S. Zaleski, "Volume-of-fluid interface tracking with smoothed surface stress methods for three-dimensional flows," J. Comput. Phys. **152**, 423 (1999).
[45]C. A. Schneider, W. S. Rasband, and K. W. Eliceiri, "NIH image to ImageJ: 25 years of image analysis," Nat. Methods **9**, 671 (2012).
[46]F. H. Harlow and J. E. Welch, "Numerical calculation of time-dependent viscous incompressible flow of fluid with free surface," Phys. Fluids **8**, 2182 (1965).
[47]W. E. Johnson, "Development and application of computer programs related to hypervelocity impact," Systems Science, and Software Report No. 3SR-353, 1970.
[48]P. K. Notz, A. U. Chen, and O. A. Basaran, "Satellite drops: Unexpected dynamics and change of scaling during pinch-off," Phys. Fluids **13**, 549 (2001).
[49]Y.-J. Chen and P. Steen, "Dynamics of inviscid capillary breakup: Collapse and pinchoff of a film bridge," J. Fluid Mech. **341**, 245 (1997).
[50]R. F. Day, E. J. Hinch, and J. R. Lister, "Self-similar capillary pinchoff of an inviscid fluid," Phys. Rev. Lett. **80**, 704 (1998).
[51]J. R. Castrejón-Pita, A. A. Castrejón-Pita, S. S. Thete, K. Sambath, I. M. Hutchings, J. Hinch, J. R. Lister, and O. A. Basaran, "Plethora of transitions during breakup of liquid filaments," Proc. Natl. Acad. Sci. U. S. A. **112**, 4582 (2015).
[52]J. Castrejón-Pita, A. Castrejón-Pita, E. Hinch, J. Lister, and I. M. Hutchings, "Self-similar breakup of near-inviscid liquids," Phys. Rev. E **86**, 015301 (2012).
[53]Y. Amarouchene, D. Bonn, J. Meunier, and H. Kellay, "Inhibition of the finite-time singularity during droplet fission of a polymeric fluid," Phys. Rev. Lett. **86**, 3558 (2001).
[54]A. U. Chen, P. K. Notz, and O. A. Basaran, "Computational and experimental analysis of pinch-off and scaling," Phys. Rev. Lett. **88**, 174501 (2002).
[55]L. Campo-Deano and C. Clasen, "The slow retraction method (SRM) for the determination of ultra-short relaxation times in capillary breakup extensional rheometry experiments," J. Non-Newtonian Fluid Mech. **165**, 1688 (2010).
[56]D. C. Vadillo, W. Mathues, and C. Clasen, "Microsecond relaxation processes in shear and extensional flows of weakly elastic polymer solutions," Rheol. Acta **51**, 755 (2012).
[57]L. E. Rodd, T. P. Scott, J. J. Cooper-White, and G. H. McKinley, "Capillary break-up rheometry of low-viscosity elastic fluids," Appl. Rheol. **15**, 12 (2005).
[58]C. Wagner, Y. Amarouchene, D. Bonn, and J. Eggers, "Droplet detachment and satellite bead formation in viscoelastic fluids," Phys. Rev. Lett. **95**, 164504 (2005).
[59]J. J. Cooper-White, J. E. Fagan, V. Tirtaatmadja, D. R. Lester, and D. V. Boger, "Drop formation dynamics of constant low-viscosity, elastic fluids," J. Non-Newtonian Fluid Mech. **106**, 29 (2002).
[60]D. T. Papageorgiou, "On the breakup of viscous-liquid threads," Phys. Fluids **7**, 1529 (1995).
[61]G. H. McKinley and A. Tripathi, "How to extract the Newtonian viscosity from capillary breakup measurements in a filament rheometer," J. Rheol. **44**, 653 (2000).

[62]V. Sharma, A. M. Ardekani, and G. H. McKinley, "'Beads on a string' structures and extensional rheometry using jet break-up," in *5th Pacific Rim Conference on Rheology* (PRCR-5), Japan, August 2010.
[63]W. Mathues, S. Formenti, C. McIlroy, O. G. Harlen, and C. Clasen, "CaBER vs ROJER-Different time scales for the thinning of a weakly elastic jet," J. Rheol. **62**, 1135 (2018).
[64]K. W. Hsiao, J. Dinic, Y. Ren, V. Sharma, and C. M. Schroeder, "Passive nonlinear microrheology for determining extensional viscosity," Phys. Fluids **29**, 121603 (2017).
[65]K. A. Marshall, A. M. Liedtke, A. H. Todt, and T. W. Walker, "Extensional rheometry with a handheld mobile device," Exp. Fluids **58**, 69 (2017).
[66]S. Sur and J. Rothstein, "Drop breakup dynamics of dilute polymer solutions: Effect of molecular weight, concentration, and viscosity," J. Rheol. **62**, 1245 (2018).
[67]A. Bazilevsky, V. Entov, and A. Rozhkov, *Liquid Filament Microrheometer and Some of its Applications* (Elsevier, Edinburgh, UK, 1990).
[68]A. V. Bazilevsky, V. M. Entov, and A. N. Rozhkov, "Breakup of a liquid bridge as a method of rheological testing of biological fluids," Fluid Dyn. **46**, 613 (2011).
[69]R. F. Liang and M. R. Mackley, "Rheological characterization of the time and strain dependence for polyisobutylene solutions," J. Non-Newtonian Fluid Mech. **52**, 387 (1994).
[70]P. Erni, M. Varagnat, C. Clasen, J. Crest, and G. H. McKinley, "Microrheometry of sub-nanolitre biopolymer samples: non-Newtonian flow phenomena of carnivorous plant mucilage," Soft Matter **7**, 10889 (2011).
[71]D. C. Vadillo, T. R. Tuladhar, A. C. Mulji, S. Jung, S. D. Hoath, and M. R. Mackley, "Evaluation of the inkjet fluid's performance using the 'Cambridge Trimaster' filament stretch and break-up device," J. Rheol. **54**, 261 (2010).
[72]P. Calvert, "Inkjet printing for materials and devices," Chem. Mater. **13**, 3299 (2001).
[73]Y. Luo, D. Zhai, Z. Huan, H. Zhu, L. Xia, J. Chang, and C. Wu, "Three-dimensional printing of hollow-struts-packed bioceramic scaffolds for bone regeneration," ACS Appl. Mater. Interfaces **7**, 24377 (2015).
[74]S. V. Murphy and A. Atala, "3D bioprinting of tissues and organs," Nat. Biotechnol. **32**, 773 (2014).
[75]C. N. Hoth, P. Schilinsky, S. A. Choulis, S. Balasubramanian, and C. J. Brabec, *Solution-Processed Organic Photovoltaics* (Springer, 2013).